

Testing Stationarity of Brain Functional Connectivity Using Change-Point Detection in fMRI Data

Mengyu Dai¹, Zhengwu Zhang² and Anuj Srivastava¹

¹Department of Statistics, Florida State University, Tallahassee, FL

²Statistical and Applied Mathematical Sciences Institute, Research Triangle Park, NC

Abstract

This paper studies two questions: (1) Does the functional connectivity (FC) in a human brain remain stationary during performance of a task? (2) If it is non-stationary, how can one evaluate and estimate dynamic FC? The framework presented here relies on pre-segmented brain regions to represent instantaneous FC as symmetric, positive-definite matrices (SPDMs), with entries denoting covariances of fMRI signals across regions. The time series of such SPDMs is tested for change point detection using two important ideas: (1) a convenient Riemannian structure on the space of SPDMs for calculating geodesic distances and sample statistics, and (2) a graph-based approach, for testing similarity of distributions, that uses pairwise distances and a minimal spanning tree. This hypothesis test results in a temporal segmentation of observation interval into parts with stationary connectivity and an estimation of graph displaying FC during each such interval. We demonstrate these ideas using fMRI data from HCP database.

1. Introduction

This paper investigates the dynamic nature of functional connectivity (FC) between different anatomical parts of brain during performances of cognitive tasks. Friston [1] defines FC as *statistical dependencies among remote neurophysiological events*. It further states that “effective connectivity is dynamic (activity-dependent), and depends on a model of interactions or coupling”. FC is usually expressed as quantification of similarity, or *correlations*, between functional measurements of neuronal activities across regions in human brain. For instance, it can be estimated using localized neuronal responses to external stimuli, as measured using different modalities. The primary tool for recording FC is functional Magnetic Resonance Imaging

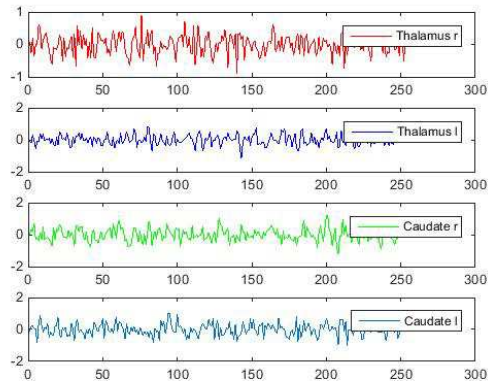


Figure 1. BOLD signals of 4 regions under the task “gambling”.

(fMRI), which measures the blood oxygen level dependent (BOLD) contrast signals of each brain voxel over a period of time. Consequently, FC can be expressed as correlation or covariance of these BOLD signals. The fMRI data used in this article is from Human Connectome Project (HCP), and an example is shown in Fig. 1. While earlier models have assumed stationary models for FC (i.e. the underlying distribution remains the same), recently there has been an increased interest in understanding changes in FC patterns during fMRI experiments. A dynamical FC model is bound to provide insight into the fundamental working mechanics of brain networks and their evolutions during performances of tasks [2]. Such a model can, for instance, be related to different neurological disorders, and has been suggested to be a more accurate representation of functional brain networks. This applies to both resting state and task-related studies.

1.1. Past Work on FC Dynamics

For a review of recent progress on analyzing FC, please refer to [1, 3]. A majority of early work assumed stationary FC, but recently some studies have developed tests for changes in coherence pattern of multiple regions of interest (ROI) [4]. For instance, Dynamic Connectivity Regression (DCR) is a data-driven technique used for detecting temporal change points in FC between brain regions, where the number and location of the change points are unknown a priori. A new DCR algorithm involving single-subject data is introduced in [5]. This algorithm increases accuracy with a small number of observations and reduces the number of false positives in the estimated undirected (connectivity) graphs. Dynamic connectivity detection builds upon the framework of a DCR algorithm. It overcomes the shortcomings of DCR by adopting a simplified sparse matrix estimation approach and a different hypothesis testing procedure to determine change points [6]. In case FC is represented by a correlation matrix of fMRI signals recorded at different locations, a sliding (time) window technique is often used to estimate the correlation matrix. Lindquist et al. [2] critique the sliding-window technique, and discuss some alternative methods that have been used to model financial volatility in the past. Similar to [7], where an asymptotic test procedure to assess the stability of volatility and cross-volatility of linear and nonlinear multivariate time series models is introduced, they use a hypothesis test but with neuro-imaging data.

1.2. Our Approach

We analyze stationarity of FC by developing a formal statistical test. We start by taking a fixed partitioning of human brain into functional units or regions. Then, we represent the instantaneous FC as a symmetric, positive definite matrix (SPDM) with entries denoting covariances of localized functional responses under resting state or under external stimuli. In this computation, we use a sliding window to segment multivariate time series into overlapping blocks, and compute a covariance matrix for each block. The original time series data (BOLD signal) can thus be converted into an indexed sequence of SPDMs and the goal is now to detect if these matrices denote samples from a single distribution or the underlying distribution changes at some time points. In other words, we formulate the question of testing stationarity of FC as a problem of change-point detection in the associated SPDM process. The actual test is performed using the graphical approach of Chen et al. [8], where one constructs a minimal spanning tree (MST) connecting the observed SPDMs. The number of edges connecting across temporally divided subgroups leads to a test statistic for change point detection. We utilize a Riemannian structure on the space of SPDMs to define and compute geodesic dis-

tances between covariance matrices, and to facilitate construction of MSTs.

The rest of this paper is as follows. In Section 2, we describe components of our proposed framework, including: representation of FC using covariance matrices, the Riemannian structure on space of SPDMs, a graphical approach for detecting change points, and a method for reconstructing connectivity in homogeneous time periods. Section 3 outlines the overall estimation procedure and Section 4 presents some experimental results using HCP fMRI data.

2. Components of the Proposed Framework

The proposed framework for detecting change point in FC, during the performance of a task, is made up of several current and novel components. In this section we briefly outline these parts.

2.1. Covariance Estimation

The first problem is to estimate a correlation or a covariance matrix that represents the functional connectivity between anatomical parts in brain. To specify this matrix, we segment the brain anatomy into d regions and then represent the functional connectivity at any time using a $d \times d$ covariance matrix of corresponding BOLD signals. In this paper we take a simple approach and use the standard sample covariance matrix of signal over a temporal window. (There are more sophisticated ways of estimating covariance matrix, see for example [9], and those can easily be applied here.) We segment multivariate time series into overlapping blocks with equal sizes. The block-size should be large enough to result in a positive definite covariance, but not too large to smooth over the subtle changes that are critical to assess stationarity of FC. Additionally, the step size for moving the window should be large enough to reduce dependency in successive covariance matrices. If the step is too small, then only few points differ in successive blocks, and the estimated covariance matrix will not change significantly over time. In the experiments presented later, we use a step-size to window-size ratio that is at least 0.2. If the fMRI signal at location j is denoted by $X_j(t) \in \mathbb{R}$, then the sample covariance matrix is a $d \times d$ matrix with (j, k) entry: $P_{jk} = \frac{1}{T-1} \sum_{i=1}^T (X_j(t) - \bar{X}_j) (X_k(t) - \bar{X}_k)$, where $\bar{X}_j(t) = \frac{1}{T} \sum_{t=1}^T X_j(t)$.

2.2. Riemannian Structure on SPDMs

In order to evaluate stationarity of covariance matrices over observation periods, we need impose a metric structure on the space of SPDMs. While there are several Riemannian and metric structures used in the literature, including [10], we briefly summarize a convenient Riemannian structure taken from [11, 12]; please refer to these papers for details.

Let \mathcal{P} be the space of $n \times n$ SPDMS, and let $\tilde{\mathcal{P}}$ be its subset of matrices with determinant one. Recall that for any $G \in SL(n)$, one can decompose it uniquely as $G = PS$ where $P \in \tilde{\mathcal{P}}$ and $S \in SO(n)$. The quotient space $SL(n)/SO(n)$ is the set of all orbits of the type $[G] = \{GS | S \in SO(n)\}$, for $G \in SL(n)$. Thus, we can identify $\tilde{\mathcal{P}}$ with the quotient space $SL(n)/SO(n)$ via a map $\pi : SL(n)/SO(n) \rightarrow \tilde{\mathcal{P}}$, given by $\pi([G]) = \sqrt{\tilde{G}\tilde{G}^t}$, for any $\tilde{G} \in [G]$. One can verify that $\pi([G])$ lies in $\tilde{\mathcal{P}}$ by letting $\tilde{G} = \tilde{P}S$ (polar decomposition), and then $\pi([G]) = \sqrt{\tilde{G}\tilde{G}^t} = \sqrt{\tilde{P}S S^t \tilde{P}} = \tilde{P}$. The inverse map of π is given by: $\pi^{-1}(\tilde{P}) = [\tilde{P}] \equiv \{\tilde{P}S | S \in SO(n)\} \in SL(n)/SO(n)$. This establishes a one-to-one correspondence between the quotient space $SL(n)/SO(n)$ and $\tilde{\mathcal{P}}$.

There are several other bijections between these sets, including the mapping proposed by Pennec et al. [10]: $\pi_B([G]) = \tilde{G}\tilde{G}^T$ with the inverse $\pi_B^{-1}(\tilde{P}) = [\sqrt{\tilde{P}}]$. If we use π_B to transfer the Riemannian structure from the quotient space $SL(n)/SO(n)$ onto $\tilde{\mathcal{P}}$, we will reach the one used in earlier papers [10]. However, π gives us convenient formulae (parallel transport, exponential map, inverse exponential map, etc) for statistical analysis of elements in $\tilde{\mathcal{P}}$, and thus we choose to use π here.

Now, we start with a natural Riemannian metric on $SL(n)$, the trace metric, and use the map π to push it forward from the quotient space $SL(n)/SO(n)$ to $\tilde{\mathcal{P}}$. This process leads to the following geodesic distance in $\tilde{\mathcal{P}}$. For any $\tilde{P}_1, \tilde{P}_2 \in \tilde{\mathcal{P}}$, $d_{\tilde{\mathcal{P}}}(\tilde{P}_1, \tilde{P}_2) = \|A_{12}\|$ where $A_{12} = \log(P_{12})$ and $P_{12} = \sqrt{\tilde{P}_1^{-1}\tilde{P}_2\tilde{P}_1^{-1}}$. Reader can refer to [12] for more details of this metric. Next, we extend this Riemannian structure to \mathcal{P} , the space of SPDMS. Since for any $P \in \mathcal{P}$ we have $\det(P) > 0$, we can express $P = (\tilde{P}, \frac{1}{n} \log(\det(P)))$ with $\tilde{P} = \frac{P}{\det(P)^{1/n}} \in \tilde{\mathcal{P}}$. Thus, \mathcal{P} is identified with the product space of $\tilde{\mathcal{P}} \times \mathbb{R}$ and we take a weighted combinations of distances on these components to reach a metric on $\tilde{\mathcal{P}}$ is: $d_{\mathcal{P}}(I, P)^2 = d_{\tilde{\mathcal{P}}}(I, \tilde{P})^2 + \frac{1}{n} (\log(\det(P)))^2$. Finally, for two SPDMS P_1 and P_2 , let $P_{12} = P_1^{-1}P_2S_{12} \in \mathcal{P}$ for some $S_{12} \in SO(n)$. Then, we have $\det(P_{12}) = \det(P_2)/\det(P_1)$. Therefore, the resulting squared geodesic distance between two SPDMS P_1 and P_2 is $d_{\mathcal{P}}(P_1, P_2)^2 = d_{\tilde{\mathcal{P}}}(I, P_{12})^2 + \frac{1}{n} (\log(\det(P_2)) - \log(\det(P_1)))^2$.

Once we have a distance on SPDMS, we can use it to define and compute sample means on \mathcal{P} as follows. The sample Karcher mean of a given set of SPDMS is given by $\mu_{\mathcal{P}} = \arg \min_{P \in \mathcal{P}} \sum_{i=1}^n (d_{\mathcal{P}}(P, P_i))^2$, P_i denotes the i -th SPDMS. The algorithm for computing Karcher mean is a standard one and is not repeated here. We refer the reader to [11, 12] for those details.

2.3. Change-Point Detection Using MST

The next issue is to detect change points in the underlying distribution associated with a time series, using a distance-based approach. In this section we summarize the approach introduced by Chen and Zhang in [8] for solving this problem. We note that Friedman and Rafsky in [13] proposed the first graph-based test for testing the null hypothesis that subjects from two groups are equal in distribution. Then, Chen and Nancy Zhang in [8] adapted this framework to change-point detection of times series on arbitrary metric spaces.

The basic formulation is as follows: Let X_1, X_2, \dots, X_T be random variables taking values on a manifold M , and let F_0, F_1 denote different probability distribution functions on M . We are interested in testing the null hypothesis that all X_t s are samples from the same distribution, against an alternative that all points after a certain time τ follow a different distribution. That is,

$$\begin{aligned} H_0 : & \quad X_t \sim F_0, \quad t = 1, 2, \dots, T \\ H_1 : & \quad \exists 1 \leq \tau < T, \quad X_t \sim \begin{cases} F_1, & t \leq \tau \\ F_0, & \text{otherwise} \end{cases} \end{aligned}$$

This test is phrased for a single change point, at time τ , but one can perform this test for different τ s to find multiple change points.

The test statistic $Z(\tau)$ is calculated as follows. First we compute all the pairwise distances between all X_t under the chosen metric on M . Then, we use these pairwise distances to form a minimal spanning tree (MST) connecting these points. An MST is a connected graph such that: (1) each X_t is a node in the graph, (2) if any two points are connected by an edge then the weight of that edge is given by the pairwise distance between those points, and (3) the sum of weights of all connected edges is the smallest amongst all such graphs. (We note that the MST is independent of the ordering of the given points.) To test, if there is a change point at a $\tau \in \{1, 2, \dots, T-1\}$, we divide X_t s into two groups: $\{X_1, \dots, X_\tau\}$, and $\{X_{\tau+1}, \dots, X_T\}$. Let $R(\tau)$ represents the number of edges that connect points across two groups in MST. Intuitively, if τ is a change point then this separation represents an appropriate clustering of points and only a small number of edges connect across those clusters. In contrast, if the two groups are from the same distribution, then we expect a large number of edges in MST going across the groups.

In order to evaluate the size of $R(\tau)$ we use a bootstrap approach as follows. We randomly divide the full set of points into two groups of size τ and $(T - \tau)$, and count the number of cross edges; call it $R_b(\tau)$. This is a bootstrap replicate of $R(\tau)$. We compute these replicates $\{R_b(\tau) | b = 1, 2, \dots, B\}$ and use their sample mean and standard-deviation to standardize $R(\tau)$. Let $Z(\tau) =$

$-\frac{(R(\tau) - \bar{R}(\tau))}{\hat{\sigma}_{R(\tau)}}$ be the test statistic, where $\bar{R}(\tau)$ and $\hat{\sigma}_{R(\tau)}$ are mean and standard deviations of $\{R_b(\tau)\}$. This standardized test statistic is then tested for a given confidence level for accepting or rejecting the null hypothesis. If there is a change point at τ , and if the observations are independent or weakly dependent, then a $Z(\tau) \geq 3$ implies a change-point detection at 0.95 confidence level. If $Z(\tau) \geq 4$, this implies a change point detection at 0.99 confidence level. The change-point detection algorithm is summarized as follows:

- Algorithm 1**
1. For a given ordered set of points $\{X_t \in M, t = 1, 2, \dots, T\}$, compute D , the $T \times T$ pairwise geodesic distance matrix.
 2. Use D to form a minimal spanning tree (MST) connecting all the points.
 3. For a fixed τ , count $R(\tau)$, the number of edges in this MST between first group: $\{X_1, \dots, X_\tau\}$, and the second group $\{X_{\tau+1}, \dots, X_T\}$.
 4. For $b = 1, 2, \dots, B$, repeat:
 - (a) Randomly separate the full set of points into two groups of size τ and $T - \tau$.
 - (b) Use the previous MST to compute $R_b(\tau)$, the number of edges connecting these the two groups.
 5. Use the mean and standard deviation of $\{R_b(\tau)\}$ to standardize $R(\tau)$, and compute $Z(\tau)$. If $Z(\tau) \geq 3$, a change point is detected (at 0.95 confidence level).

We illustrate this algorithm with $M = \mathcal{P}$ and the corresponding geodesic distance $d_{\mathcal{P}}$. In these examples we form a set of covariance matrices computed from zero-mean Gaussian data, simulated from either the same or different covariance matrices. We then apply Algorithm 1 and study the test statistics $Z(\tau)$. Fig. 2 shows two examples of this experiment. In the top example, the first 9 covariances were generated from one model and the remaining 10 from a different model. It can be seen that there is only one edge (drawn in red) connecting these two groups in MST. As a result, $R(\tau)$ will be small $Z(\tau)$ will be large for $\tau = 9$. In the bottom case, we generate 39 covariances matrices from the same model and randomly divide them into two groups. In this case we see a lot of edges connecting the two groups and no clear separation; thus, $R(\tau)$ will be large and $Z(\tau)$ will be small for all τ .

To test for multiple change points in a time sequence of SPDMS, we can repeatedly use the same idea but only after localizing each test in time, using a moving window. (This window is different from and much larger than the one used for estimating covariances earlier). This is needed because

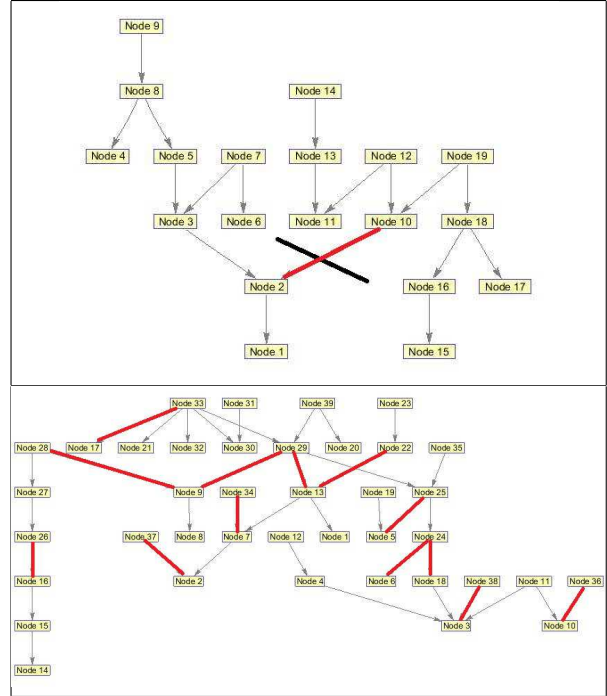


Figure 2. Top: MST involving 19 SPDMS matrices with a real change point at $\tau = 10$. The two groups are $\{1, 2, \dots, 9\}$ and $\{10, 11, \dots, 19\}$. Bottom: MST involving 39 SPDMS matrices with no change point. The groups are formed by randomly dividing the points in two groups. The red edges represent connections across the chosen groups.

the future changes in distributions can adversely affect our ability to test for a change point at the current time. By restricting to a window we try to ensure that it contains at most one change point. We remind the reader that the hypothesis test, and the related test statistic computation, assumes that there are at most two distributions, one before τ and one after τ in the set $\{1, 2, \dots, T\}$. The presence of another change point down the line can violate that assumption. Therefore, we use a moving window to localize computations and decisions in time. Given a window of fixed length, we detect whether mid point in the window is a change point, and then slide the window. An example of moving window embedded in the distance matrix is given in Fig. 3.

2.4. Estimating Functional Connectivity

Given a covariance matrix, denoting stationary FC over a sub-interval, we are interested in estimating and visualizing a graph representing the connectivity of different brain regions. We accomplish that by using a graphical Lasso based method introduced in [14]. Let the observation period $[0, T]$ be subdivided into several sub-intervals by detected change points at τ_1, τ_2 , etc. For each sub-interval $[\tau_j, \tau_{j+1}]$

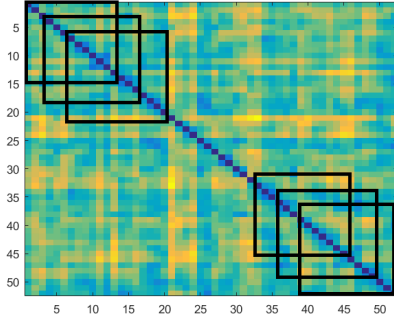


Figure 3. A moving window for localizing change point detection, over a 52×52 distance matrix.

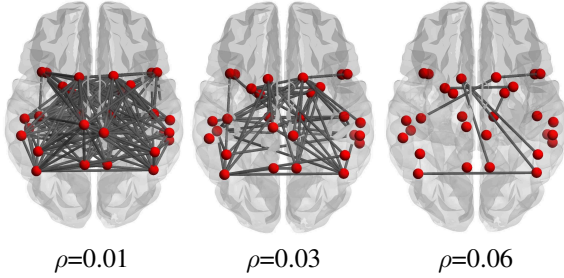


Figure 4. Estimated connectivity of 30 ROIs using the same covariance but different ρ .

we compute the Karcher mean of all SPDMs over this sub-interval; call it $\bar{P}_j \in \mathcal{P}$. Then, we use this average SPDM to estimate the associated precision matrix $\Theta = \bar{P}_j^{-1}$ by:

$$\hat{\Theta}_j = \underset{\Theta \geq 0}{\operatorname{argmin}} (tr(\bar{P}_j \Theta) - \log \det(\Theta) + \rho \sum_{i \neq k} |\Theta_{ik}|). \quad (1)$$

where $\rho > 0$ is a parameter controls density of the generated graph (Fig. 4 illustrates its effect). While $\rho > 0$ increases, the adjacency matrix becomes more sparse. Given the estimated precision matrix $\hat{\Theta}_i$, the adjacency matrix is identified as $(A_j)_{ik} = 1_{|\hat{\Theta}_{ik}| \neq 0}$. This adjacency matrix is then used to form an undirected graph formed by the corresponding brain regions.

3. Overall Procedure

We summarize the overall procedure for detecting change points in FC observations and for estimating connectivity graphs during homogeneous sub-intervals. In the following: T denotes the full observation period, W denotes the size of a time window for computing covariance matrices, S is the step size for sliding W - windows, and T_0 is the size of a square-block of the distance matrix for localizing change-point test. As an example, in one experiment we have $T = 52$, $W = 15$, $S = 5$, and $T_0 = 25$.

Algorithm 2 Given a segmentation of brain into functional units or anatomical regions of interest.

1. Divide the fMRI data into T different time blocks, and compute covariances of BOLD signals in each time block using sliding windows of width W and step size S ($0.2W \leq S < W$), resulting in $\{P_1, P_2, \dots, P_T\}$.
2. Compute $T \times T$ pairwise distance matrix between these covariances.
3. For each $T_0 \times T_0$ diagonal block in the distance matrix (with $T_0 < T$), perform the following:
 - (a) Use Algorithm 1, to form a normalized test statistic $Z(\tau)$, where $\tau = T_0/2$.
 - (b) Select the τ if $Z(\tau) > 3$ as a change-points of FC.

Let the set of selected change points be $\{\tau_j\}$

4. For each sub-interval $\{\tau_j, \tau_{j+1}\}$, find the Karcher mean of covariance matrices $\{P_{\tau_j}, P_{\tau_j+1}, \dots, P_{\tau_{j+1}}\}$ to form \bar{P}_j .
5. For each \bar{P}_j , estimate its precisions matrix using Eqn. 1 and the the corresponding adjacency matrix to represent its connectivity graph.

4. Experiments

In this section we demonstrate the algorithm using both simulated and real fMRI datasets.

4.1. Simulation Study

In the first experiment, we simulate a d -dimensional time sequence data with $T = 900$ sample points from 3 different multivariate normal distributions. Data points from $t = 1$ to $t = 300$ are simulated from $f_1(\mu_1, \Sigma_1)$, from $t = 301$ to $t = 600$ are from $f_2(\mu_2, \Sigma_2)$, and from $t = 601$ to $t = 900$ are from $f_3(\mu_3, \Sigma_3)$, where $\mu_1 = \mu_2 = \mu_3 = \mathbf{0}$, and Σ_1, Σ_2 and Σ_3 are randomly generated in such a way that $d_{\bar{P}}(\Sigma_i, \Sigma_{i+1}) > 0.6$.

To detect change points we implemented Algorithm 2 using $W = 30$, $S = 20$ and $T_0 = 25$, where W stands for the window size and S represents step size of sliding windows. Fig. 5 shows a plot of the test statistic $Z(\tau)$ versus τ , for $d = 2$ in the left panel and $d = 10$ in the right panel. The detected change points are marked using black circles, and one can clearly see the peak value of test statistic around the detected change points, and this agrees with the true change points in the simulated datasets.

4.2. Real Data Study

Now we take the task fMRI (tfMRI) data from Human Connectome Project (HCP) [15] to study the dynamic functional connectivity (FC) problem. The majority of the HCP

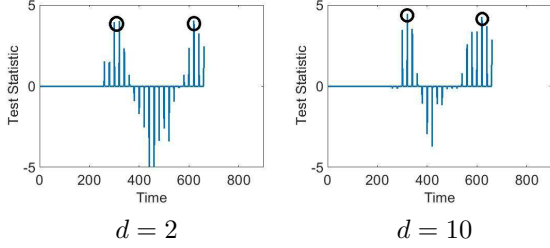


Figure 5. Change point detection result for two simulated data. Detected change points are marked using black circles.

tfMRI data were acquired at 3T, which is considered to be the field strength currently most suitable for acquiring high quality data reliably from a large cohort of subjects. Acquisitions are based on blood oxygen level dependent (BOLD) contrast. A series of 4D imaging data were acquired for each subject while the subjects perform different tasks involving different neural systems, e.g. visual, motion and cognition systems. The acquired image is with an isometric spatial resolution of 2 mm and temporal resolution of 2 s. All fMRI data in HCP are preprocessed by removing spatial distortions, realigning volume to compensate for subject motion, registering the fMRI to the structural MRI, reducing the bias field, normalizing the 4D image to a global mean, masking the data with the final brain mask and aligning the brain to a standard space [16]. This preprocessed tfMRI is then available for connectivity analysis.

To map functional connectivity, we begin with the segmentation of brain into regions using an existing template, such as the AAL (Automated Anatomical Labeling) atlas [17]. Time series for each region in tfMRI are extracted using CONN functional connectivity toolbox [18] and AAL atlas (116 regions). A $[0.008, \infty]$ (Hz) high-pass filter is used to de-noise the functional data. Fig. 1 shows one example of the de-noised BOLD signals of 4 regions from a subject in HCP.

Next, we evaluate the dynamic FC using the proposed method in two different tasks: (1) gambling and (2) social cognition.

4.2.1 Dynamic FC for Gambling Task

The gambling task in HCP was adapted from the one developed in [19]. Participants play a card guessing game where they are asked to guess the number on a mystery card in order to win or loss money. Three different blocks are presented through out the task: reward blocks, neutral blocks and loss blocks. Brain regions that relate to this task include basal ganglia, ventral medial prefrontal and orbito-frontal. The basal ganglia contains multiple subcortical nuclei and is the part of brain that influences motivation and action selection.

In the first study, we selected four regions inside the

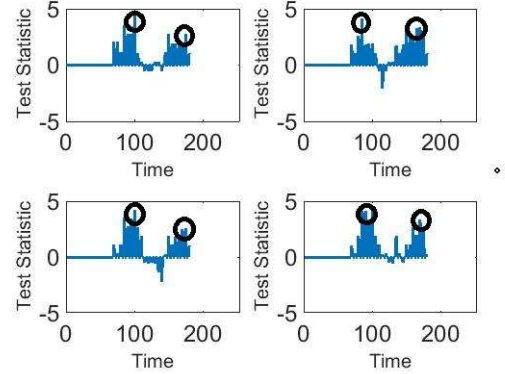
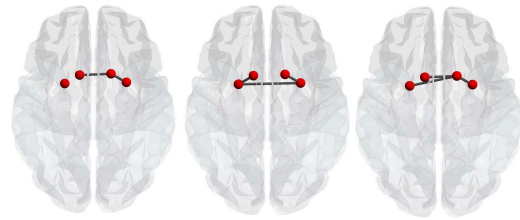


Figure 6. FC change point detection for four regions in basal ganglia in gambling task with difference window sizes and $T_0 = 25$



Sub-interval 1 Sub-interval 2 Sub-interval 3
Figure 7. Reconstructed connectivity for four nodes in basal ganglia region through out the gambling task.

basal ganglia: right & left Caudate and right & left Putamen, and study FC using 4×4 SPDMs representing covariance of fMRI signal in these four regions. Algorithm 1 is applied and the results are shown in Fig. 6. It shows the evolution of the test statistic versus τ for four different choices of window size W (from top-left to bottom-right, the window sizes used are 15, 16, 17 and 18 respectively). Despite different window sizes, the Algorithm consistently detects two change points, which means these four nodes formed three different connection patterns during the task. Moreover, we reconstructed the network structures for the four regions in basal ganglia using tfMRI data in the 3 intervals segmented by the two detected change points. The reconstructed three different network structures are presented in Fig. 7.

In the second experiment, we selected grey matter regions closed to basal ganglia (right & left central Opercular Cortex, right & left Parietal Operculum Cortex, right & left Planum Polare and right & left Heschl’s Gyrus) and estimated their connectivity pattern. These regions also have the same change point patterns. These results are consistent with the design of the task with three conditions: neutral blocks, reward blocks and loss blocks.

As a comparison we perform the change point detection for FC involving regions that are deemed irrelevant to the gambling task, e.g. Inferior Frontal Gyrus and Temporal

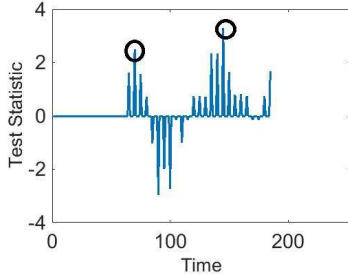


Figure 8. FC change point detection for grey matter regions near basal ganglia. $W = 14$ and $T_0 = 25$ were used.

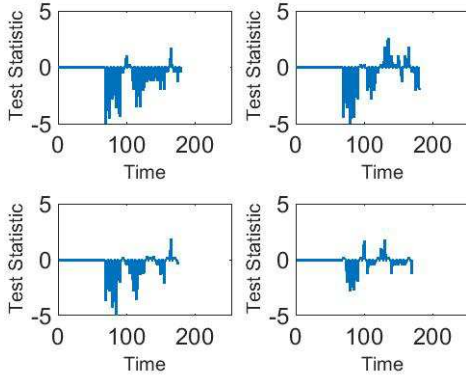


Figure 9. FC change point detection for two regions: Inferior Frontal Gyrus and right Temporal Pole with different W 's and $T_0 = 25$.

Pole Right. The result is shown in Fig. 9 and no change point in FC is detected.

4.2.2 Dynamic FC for Social Cognition Task

In this experiment, participants were presented with short video clips of objects (squares, circles, triangles) that either interacted in some way, or moved randomly on the screen [20]. After each video clip, participants judge whether the objects had (1) a mental interaction (an interaction that appears as if the shapes are taking into account each other's feeling and thoughts); (2) not sure or (3) no interaction. Each run of the task has 5 video blocks (2 Mental and 3 Random in the data we used). Possible brain regions that relate to this task are medial prefrontal cortex, temporal parietal junction, inferior and superior temporal sulcus [21]. Since this task has more experimental blocks (5 blocks) than the gambling data, we expect to detect more change points.

Fig. 10 shows the results of Algorithm 2 on this data using four regions inside the inferior frontal gyrus. The algorithm detects 4 change points, implying that the functional network structure changes frequently during the task. In another example, using 14 regions instead, the algorithm detects the change point of the connectivity formed by these

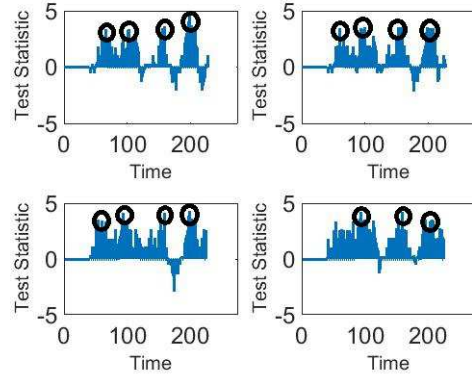


Figure 10. FC change point detection result in social cognition task for 4 regions of the inferior frontal gyrus with different W 's and $T_0 = 25$.

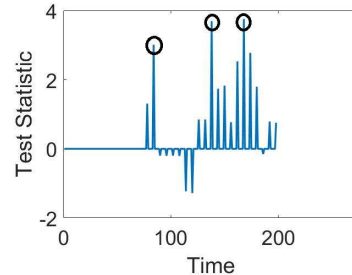


Figure 11. FC change point detection in social cognition task for 14 regions (ROI 50-63) in AAL atlas for $W = 16$ and $T_0 = 25$.

regions. Fig. 11 shows the result using block size 18. Three major change points are detected in these regions. We reconstruct the connectivity networks for the 14 ROIs using data in the four sub-intervals defined by the three detected change points. Fig. 12 shows the reconstructed networks.

5. Conclusion

This paper describes a statistical approach for testing stationarity of functional connectivity between brain regions, during execution of certain tasks. In this approach, instantaneous FC is represented by a matrix of covariances between signals observed at different regions, and one obtains a time-series of SPDMs for each task. This sequence is then tested for change-point detection using a graphical approach that utilizes a Riemannian structure on SPDMs to compute distances and means. This detection divides the observation interval into sub-intervals with stationary connectivity patterns. We average the SPDMs in each interval, form a precision matrix for each average, and threshold it to compute and display connectivity patterns for each sub-interval. This framework provides tools for studying dynamical FC patterns under different tasks for different subjects.

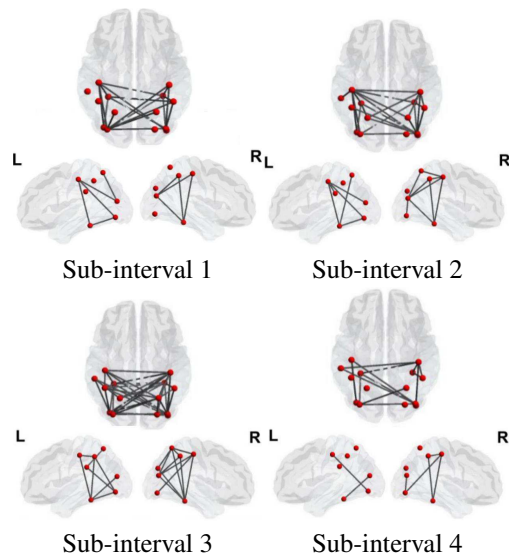


Figure 12. Reconstructed FC network for 14 regions (50-63) in AAL atlas.

6. Acknowledgment

Data in this paper were provided by the Human Connectome Project, WU-Minn Consortium (Principal Investigators: David Van Essen and Kamil Ugurbil; 1U54MH091657) funded by the 16 NIH Institutes and Centers that support the NIH Blueprint for Neuroscience Research; and by the McDonnell Center for Systems Neuroscience at Washington University.

This research was supported in part by NSF CCF-1319658 and NSF IIS-1342109.

References

- [1] K. J. Friston. Functional and effective connectivity: A review. *Brain Connectivity*, 1(1):13–36, 2011.
- [2] M. Lindquist, Y. Xu, M. Nebel, and B. Caffo. Evaluating dynamic bivariate correlations in resting-state fmri: A comparison study and a new approach. *NeuroImage*, 101:531 – 546, 2014.
- [3] R. M. Hutchison et al. Dynamic functional connectivity: Promise, issues, and interpretations. *NeuroImage*, 80:360–378, 2013.
- [4] R. A. Poldrack. Region of interest analysis for fmri. *Social Cognitive and Affective Neuroscience*, 2(1):67–70, 2007.
- [5] I. Cribben, T. Wager, and M. Lindquist. Detecting functional connectivity change points for single-subject fmri data. *Frontiers in Computational Neuroscience*, 7(143), 2013.
- [6] Y. Xu and M. A Lindquist. Dynamic connectivity detection: an algorithm for determining functional connectivity change points in fmri data. *Frontiers in Neuroscience*, 9(285), 2015.
- [7] A. Aue, S. Hormann, L. Horvath, and M. Reimherr. Break detection in the covariance structure of multivariate timeseries models. *The Annals of Statistics*, 37(6B), 2009.
- [8] H. Chen and N. Zhang. Graph-based change-point detection. *Ann. Statist.*, 43(1):139–176, 02 2015.
- [9] M. Hinne, R. J. Janssen, T. Heskes, and M. A. van Gerven. Bayesian estimation of conditional independence graphs improves functional connectivity estimates. *PLoS Comput Biol*, 11(11):e1004534, 2015.
- [10] X. Pennec, P. Fillard, and N. Ayache. A Riemannian framework for tensor computing. *Int. J. Comput. Vision*, 66(1):41–66, 2006.
- [11] J. Su, I. L. Dryden, E. Klassen, H. Le, and A. Srivastava. Fitting optimal curves to time-indexed, noisy observations on nonlinear manifolds. *Journal of Image and Vision Computing*, 30(6-7):428–442, 2012.
- [12] Z. Zhang, J. Su, E. Klassen, H. Le, and A. Srivastava. Video-based action recognition using rate-invariant analysis of covariance trajectories. *IEEE Transactions on Pattern Analysis and Machine Intelligence*, in review, 2015.
- [13] J. H. Friedman and L. C. Rafsky. Multivariate generalizations of the wald-wolfowitz and smirnov two-sample tests. *Ann. Statist.*, 7(4):697–717, 07 1979.
- [14] J. Friedman, T. Hastie, and R. Tibshirani. Sparse inverse covariance estimation with the graphical lasso. *Biostatistics*, 9(3):432–441, 2008.
- [15] D. C. Van Essen and et al. The WU-Minn Human Connectome Project: An overview. *NeuroImage*, 80:62–79, 2013.
- [16] M. F. Glasser and et al. The minimal preprocessing pipelines for the Human Connectome Project. *NeuroImage*, 80:105–124, 2013.
- [17] N. Tzourio-Mazoyer, B. Landeau, D. Papathanassiou, F. Crivello, O. Etard, N. Delcroix, Bernard Mazoyer, and M. Joliot. Automated anatomical labeling of activations in spm using a macroscopic anatomical parcellation of the mni mri single-subject brain. *NeuroImage*, 15(1):273–279, January 2002.

- [18] S. Whitfield-Gabrieli and A. Nieto-Castanon. Conn: a functional connectivity toolbox for correlated and anticorrelated brain networks. *Brain Connect*, 2(3):125–141, 2012.
- [19] M. R. Delgado, L. E. Nystrom, C. Fissell, D. C. Noll, and J. A. Fiez. Tracking the hemodynamic responses to reward and punishment in the striatum. *J. Neurophysiol.*, 84(6):3072–3077, Dec 2000.
- [20] F. Castelli, F. Happ, U. Frith, and C. Frith. Movement and mind: A functional imaging study of perception and interpretation of complex intentional movement patterns. *NeuroImage*, 12(3):314 – 325, 2000.
- [21] D. M. Barch and et al. Function in the human connectome: Task-fMRI and individual differences in behavior. *NeuroImage*, 80:169–189, 2013.